A functionally personalized boundary condition model to improve estimates of fractional flow reserve with CT (CT-FFR)

Moti Freiman[a)]
Global Advanced Technology, CT BU, Advanced Technologies Center, Philips Healthcare, Building No. 34, P.O. Box 325 Haifa 3100202, Israel

Hannes Nickisch and Holger Schmitt
Philips Research Europe, Sector Medical Imaging Systems Röntgenstr. 22-24 Hamburg, DE 22315, Germany

Pál Maurovich-Horvat
MTA-SE Cardiovascular Imaging Research Group, Heart and Vascular Center, Semmelweis University, Hungary, Germany

Patrick M Donnelly
The Ulster Hospital, Dundonald, Ireland

Mani Vembar
Advanced Systems Group CT Engineering Philips Healthcare, 3262 Darien Lane Twinsburg, OH 44087, USA

Liran Goshen
Global Advanced Technology, CT BU, Advanced Technologies Center, Philips Healthcare, Building No. 34, P.O. Box 325 Haifa 3100202, Israel

(Received 9 August 2017; revised 26 December 2017; accepted for publication 29 December 2017; published xx xxxx xxxx)

Purpose: The purpose of this study is to develop and evaluate a functionally personalized boundary condition (BC) model for estimating the fractional flow reserve (FFR) from coronary computed tomography angiography (CCTA) using flow simulation (CT-FFR).
Materials and methods: The CCTA data of 90 subjects with subsequent invasive FFR in 123 lesions within 21 days (range: 0–83) were retrospectively collected. We developed a functionally personalized BC model accounting specifically for the coronary microvascular resistance dependency on the coronary outlets pressure suggested by several physiological studies. We used the proposed model to estimate the hemodynamic significance of coronary lesions with an open-loop physics-based flow simulation. We generated three-dimensional (3D) coronary tree geometries using automatic software and corrected manually where required. We evaluated the improvement in CT-FFR estimates achieved using a functionally personalized BC model over anatomically personalized BC model using k-fold cross-validation.
Results: The functionally personalized BC model slightly improved CT-FFR specificity in determining hemodynamic significance of lesions with intermediate diameter stenosis (30%–70%, N = 72), compared to the anatomically personalized model lesions with invasive FFR measurements as the reference (sensitivity/specificity: 0.882/0.79 vs 0.882/0.763). For the entire set of 123 coronary lesions, the functionally personalized BC model improved only the area under the curve (AUC) but not the sensitivity/specificity in determining the hemodynamic significance of lesions, compared to the anatomically personalized model (AUC: 0.884 vs 0.875, sensitivity/specificity: 0.848/0.805).
Conclusion: The functionally personalized BC model has the potential to improve the quality of CT-FFR estimates compared to an anatomically personalized BC model. © *2018 American Association of Physicists in Medicine* [https://doi.org/10.1002/mp.12753]

Key words: coronary computed tomography angiography, flow simulation, coronary artery disease, boundary condition model

1. INTRODUCTION

Coronary artery disease (CAD) is the most common cause of death globally, accounting for 8.14 million deaths in 2013.[1] Coronary computed tomography angiography (CCTA) is a rapidly evolving noninvasive technique to rule out CAD due to its high negative predictive value.[2] However, CCTA provides mainly an anatomical characterization of the coronary lesions rather than assessing their hemodynamic significance by means of fractional flow reserve (FFR, that is, the ratio between the pressure distal to a lesion and the aortic pressure).[3]

Recently, physics-based flow simulations were suggested to noninvasively assess the hemodynamic significance of coronary lesions from CCTA data (CT-FFR).[4,5]

Physics-based non-invasive assessment of coronary lesions' hemodynamic significance from CCTA using CT-FFR commonly consists of three main steps:

- Accurate patient-specific three-dimensional (3D) modeling of the coronary artery tree from the CCTA data;
- Assignment of personalized boundary conditions representing the underlying physiology and microvasculature that although may be possible to extract from CCTA data, may require advanced methods, and;
- Use of a numerical solver to solve the governing flow equations.

Existing algorithms[6–8] can be used to generate accurate patient-specific 3D models of the coronary tree with manual adjustment where required. Computational fluid dynamics (CFD) methods,[9,10] reduced order models[11] or learned zero-dimensional (0D) lumped models[12] can solve the governing flow equations.

Personalized boundary conditions are usually derived from physiological rules associated with patient anatomy and blood flow-related parameters,[9,13,14] but can also be derived by more careful analysis of the CCTA data such as by, for example, using contrast kinetics or structural changes.[15,16] A unique challenge in physics-based simulation of blood flow in the coronary arteries is the modeling of autoregulatory mechanisms controlling different factors influencing overall flow. Kim et al. demonstrated how to model and incorporate several autoregulatory mechanisms including the systemic arterial baroreceptors, the degree of compensatory mechanisms due to the brain vasomotor center, and the coronary flow as a response to hyperemic conditions in a closed-loop blood flow simulation.[17]

In this work, we present a functionally personalized boundary condition model (Fig. 1) accounting specifically for the additional functional dependency of the coronary microvascular resistance upon the pressure at the coronary outlets previously demonstrated in several physiological studies.[18–20]

Our model first probes the hemodynamic significance of the lesions with an anatomically personalized BC model and then accounts for autoregulated changes in microvascular resistance by introducing an additional functional dependency and its influence upon the hemodynamic significance of these lesions.

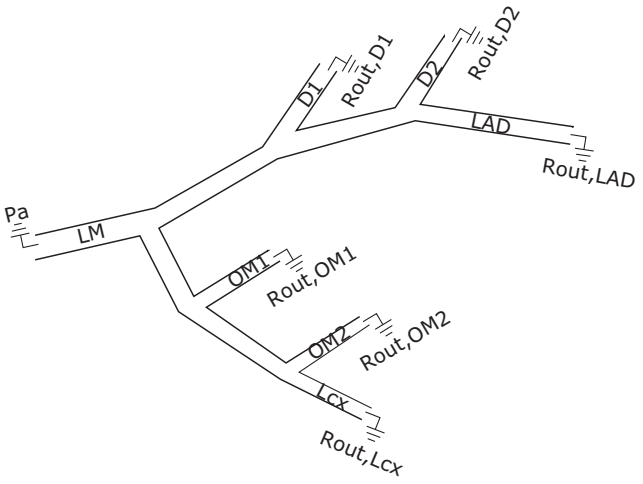

FIG. 1. Boundary condition (BC) model for our open-loop physics-based flow simulation. The inlet boundary condition represents the aortic pressure (Pa) in [$mmHg$] and the coronary outlet boundary condition represents the microvascular resistance ($R_{out,i}$) in $[g/(s \cdot cm^4)]$.

2. MATERIALS AND METHODS

2.A. Datasets

We carried out the study according to a protocol approved by the collaborating Institutional Review Boards.

Coronary computed tomography angiography data of 123 coronary lesions were retrospectively collected from 90 subjects who underwent a CCTA exam and were forwarded to invasive coronary angiography with invasive FFR measurements due to suspected CAD according to the clinical routine which was driven by qualitative CTA luminal stenosis estimation by the interpreting physician clinical symptoms. Patients with prior myocardial infarction (MI) or percutaneous coronary intervention (PCI) were excluded from the study. CCTA data were acquired using either Philips Brilliance iCT (gantry rotation time of 0.27 s) or Philips Brilliance 64 (gantry rotation time of 0.42 s). Acquisition mode was either helical retrospective ECG gating (N = 48) or prospectively gated axial scans ("Step & Shoot Cardiac") (N = 42). The kVp range was 80–140 kV and the tube output range was 600–1000 mAs for the helical retrospective scans and 200–300 mAs for the prospectively gated scans.

Table I summarizes the study population clinical data. CCTA diameter stenosis analysis (DS) performed retrospectively by an expert in CCTA image analysis (M.V., P.D., P.M.H), resulted in 72 intermediate (30%–70% DS) lesions.

Invasive FFR measurements show that 46 lesions out of the entire 123 lesions (37%) were hemodynamically significant (FFR $\leq$ 0.8). Among the subset of the 72 intermediate lesions, 34 lesions (47%) were hemodynamically significant (FFR $\leq$ 0.8).

TABLE I. Summary of study population clinical data (N = 123).

Age (years)	61.9 ± 9.8
Women	39 (32%)
Body mass index (kg/m^2)	29.6 [26.2–31.4]
Hypertension	79 (64%)
Diabetes mellitus	19 (15%)
Dyslipidaemia	89 (72%)
Smoking	32 (26%)
Day between coronary CTA and ICA	21 [0–83]
Diameter stenosis level	
<30%	48
30%–50%	37
50%–70%	35
70%–90%	3

2.B. Methods

Given a 3D mesh generated from the CCTA data with any available software dedicated for cardiac image analysis and geometrical modeling, we define the boundary conditions (BC) at a coronary outlet as follows. First, we present an anatomically personalized BC model that only accounts for anatomical variations between patients. Second, we present an improved functionally personalized BC model that accounts for both anatomical and functional variations between patients.

2.C. Anatomically personalized BC model

We model the coronary blood flow as an incompressible, Newtonian fluid with laminar flow. Assuming a healthy coronary tree with vessels segmented up to a standardized length, we model the remaining pressure differences ΔP_i^A at the different outlets to be the same for all coronaries, that is, $i \in \{LAD, D1, D2, \ldots\}$. We further base our boundary condition (BC) model on the form-follows-function scaling law described by Huo and Kassab[13] (Eqs. 2 and 4) where the volumetric flow rates at the inlet Q_{in} and at the outlets $Q_{out,i}$ are related to the respective effective radii via the following power law relation:

$$Q_{out,i} = Q_{in}\left(\frac{r_{out,i}}{r_{in}}\right)^{\frac{7}{3}} [\mathrm{cm}^3/\mathrm{s}] \tag{1}$$

By inverting this equation, pulling out the squared radii, expanding the fraction with π and the blood density ρ_{blood} in $[g/cm^3]$ and by finally introducing the definition of the outlet resistance $R_i^A = \Delta P_i^A / Q_{out,i}$, we obtain:

$$R_i^A = \frac{\Delta P_i^A \cdot \pi r_{in}^2}{Q_{in}\rho_{blood}} \cdot \frac{\rho_{blood}}{\pi r_{out,i}^2}\left(\frac{r_{in}}{r_{out,i}}\right)^{\frac{1}{3}} [g/(s \cdot cm^4)] \tag{2}$$

an expression for the outlet resistance. Since the pressure drop ΔP_i^A is assumed constant, we define the shorthand:

$$R_0 = \frac{\Delta P_i^A \cdot \pi r_{in}^2}{Q_{in}\rho_{blood}} [cm/s] \tag{3}$$

for the first term which is actually constant along the vessel and can be interpreted as the microvascular resistance.

We define an overall anatomically personalized model for assigning resistance to the coronary tree outlet by combining Eqs. 2 and 3:

$$R_i^A = \lambda \cdot \frac{\rho_{blood} R_0}{\pi r_{out,i}^2} \cdot \left(\frac{r_{in}}{r_{out,i}}\right)^{\frac{1}{3}} [g/(s \cdot cm^4)] \tag{4}$$

where λ is a unit-less anatomical personalization factor defined as:

$$\lambda = \frac{A_0}{\pi r_{in}^2} \tag{5}$$

with A_0 representing the average coronary tree inlet cross-sectional area in units of cm^2, and r_{in}^2 the patient-specific coronary tree inlet radius used to personalize the model.

We used constant values for both inlet pressure and blood density as neither can simply or at all, respectively, be obtained from CCTA data.

We learn the global model parameters R_0, A_0 by minimizing the overall sum of squared error (SSE) between the simulated FFR estimates from CCTA (FFR_{CT}) and the reference data, that is, invasively measured FFR values (FFR_{GT}) over a set of coronary lesions:

$$\widehat{R_0, A_0} = argmin_{R_0,A_0} \sum_{j=1}^{J} \left(FFR_{CT}(j, R_0, A_0) - FFR_{GT}(j)\right)^2 \tag{6}$$

where FFR_{CT} is calculated per coronary lesion j using the Lumped Model proposed by Nickisch et al.[12] with the BC model parameters R_0, A_0.

2.D. Functionally personalized BC model:

The anatomically personalized BC model (Eqs. 4 and 5) assumes a sole resistance dependency upon the patient anatomy. However, several studies demonstrated an autoregulation mechanism adjusts the microvascular resistance in response to change in the coronary outlet pressure.[19,20] We model this autoregulation mechanism by defining the target resistance at the coronary outlet as a function of patient anatomy, and the pressure at the coronary outlet:

$$R_i^F = f\left(R_i^A, p_{i,d}\right) [g/(s \cdot cm^4)] \tag{7}$$

where R_i^A is the coronary outlet resistance calculated with the anatomical model using Eqs. 4 and 5 and $p_{i,d}$ is the pressure at the outlet of coronary i.

Inspired by the inversely related correlation between the coronary outlet pressure and the microvascular resistance demonstrated by Verhoeff et al.[19] and Chamuleau et al.[20] we define this function as follows:

$$R_i^F = f\left(R_i^A, p_{i,d}\right) = R_i^A \cdot \frac{1}{\psi\left(p_{i,d}\right)} [g/(s \cdot cm^4)] \tag{8}$$

where $\psi\left(p_{i,d}\right)$ is defined as:

$$\psi\left(p_{i,d}\right) = \begin{cases} \frac{p_{i,d}}{p_a} & p_{i,d} \le p_{max} \quad [mmHg] \\ 1 & p_{i,d} > p_{max} \quad [mmHg] \end{cases} \tag{9}$$

where p_a is the aortic pressure, p_{max} represents a normal coronary outlet pressure that does not trigger the microvascular resistance autoregulation mechanism.

We use a two-phase approach to estimate R_i^F. First, we estimate R_i^A using the anatomically personalized model (Eqs. 4 and 5), and derive the value of $p_{i,d}$ from it. Next, we calculate R_i^F with Eq. 8. Figure 2 illustrates the flowchart of our functionally personalized boundary condition model.

As with the anatomically personalized model, we learn the functionally personalized model parameters R_0, A_0, p_{max} by minimizing the overall SSE between the simulated FFR

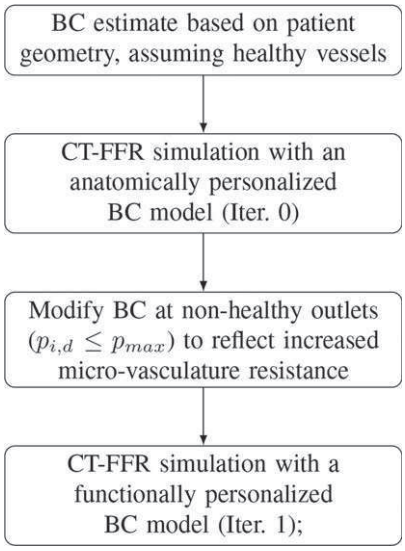

FIG. 2. Flowchart of the proposed functionally personalized boundary condition model simulation.

estimates (FFR_{CT}) and the invasively measured FFR values (FFR_{GT}) over a set of coronary lesions:

$$\widehat{R_0, A_0, p_{max}} = argmin_{R_0, A_0, p_{\max}} \sum_{j=1}^{J} \left(FFR_{CT}(j, R_0, A_0, p_{max}) - FFR_{GT}(j) \right)^2 \quad (10)$$

2.E. Physics-based open-loop lumped model flow simulation

The input to our physics-based open-loop lumped parameter model (LM) for flow simulation is a 3D coronary tree structure consisting of vessel segments linked by bifurcations.

Each vessel segment consists of a sequence of vessel cross-sections representing the varying contour and area of the coronary artery lumen. The left and right coronary artery trees are processed separately and independently of each other.

The LM simulates the physical effects causing blood pressure to change locally along the vessel including different types of friction along the vessel such as friction due to Hagen–Poiseuille's law, curvature,[21] ovality of the cross-section,[22] sudden expansion of the coronary lumen,[23] and the Bernoulli effect, which describes the conservation of energy in flows passing through cross-sections of different calibers.

The lumped model calculates local pressure changes per vessel cross-section according to the physical effects described above, which depend on a patient's individual coronary geometry.

Given the blood pressure at the inlet, the myocardial resistances at all outlets of the coronary tree model (Fig. 1), and the resistances imposed by the sequence of vessel cross-sections according to their geometry, a blood flow rate can be calculated for each vessel segment. The flow calculation is performed in analogy to electrical circuits, where changes in voltage are computed based on current and resistances. All calculations are done in a steady-state representing a mean coronary flow and pressure, such that heart cycle dependency is effectively eliminated.[12]

Once the simulation is complete, a CT-FFR value can be derived for each vessel cross-section as the ratio between the local blood pressure at and the blood pressure at the inlet of the coronary tree.

2.F. Evaluation methodology

The coronary artery centerlines and the aorta segmentation were computed automatically and adjusted manually (M.V.) to further improve the result of a commercially available software dedicated for cardiac image analysis (Comprehensive Cardiac Analysis, IntelliSpace Portal 6.0, Philips Healthcare).

We generated the 3D coronary tree model using the coronary lumen segmentation algorithm of Freiman et al.[6] with manual adjustments where required (M.V., P.M.H., P.D.).

The average user time required to generate these models including centerline extraction and lumen segmentation was 19 min (range: 8–35 min).

We estimated the hemodynamic significance of each lesion using the lumped parameter model (LM) proposed by Nickisch et al.[12] with both anatomically- and functionally personalized boundary conditions for the coronary outlets employing a globally constant ostial pressure of $p_a = 100\ mmHg$. The flow simulation computation took less than 2 s per coronary tree on a DELL T5550 Workstation equipped with 2 Intel® Xeon® ×5650 at 2.66 GHz and 40GB RAM.

We used a 10-fold cross-validation to learn both the anatomical and functional BC model parameters and estimate the CT-FFR values at the lesions using each model. Finally, we aggregated the test results from each iteration to get the model estimation results for our entire dataset.

We assessed the improvement in the CT-FFR estimates for all lesions and specifically for obstructive lesions that are considered flow-limiting based on which patients are normally sent to invasive coronary angiography (ICA) by means of root mean squared error (RMSE), mean absolute error (MAE), accuracy, bias, and 95% limits of agreement (1.96 Standard deviation) merged over the different folds.

3. RESULTS

Figure 3 presents the Bland–Altman plot of the estimated CT-FFR values using the functionally personalized (blue) and anatomically personalized (red) BC vs the invasively measured FFR values. For the entire set of lesions, the functionally personalized BC model reduces the overall bias by

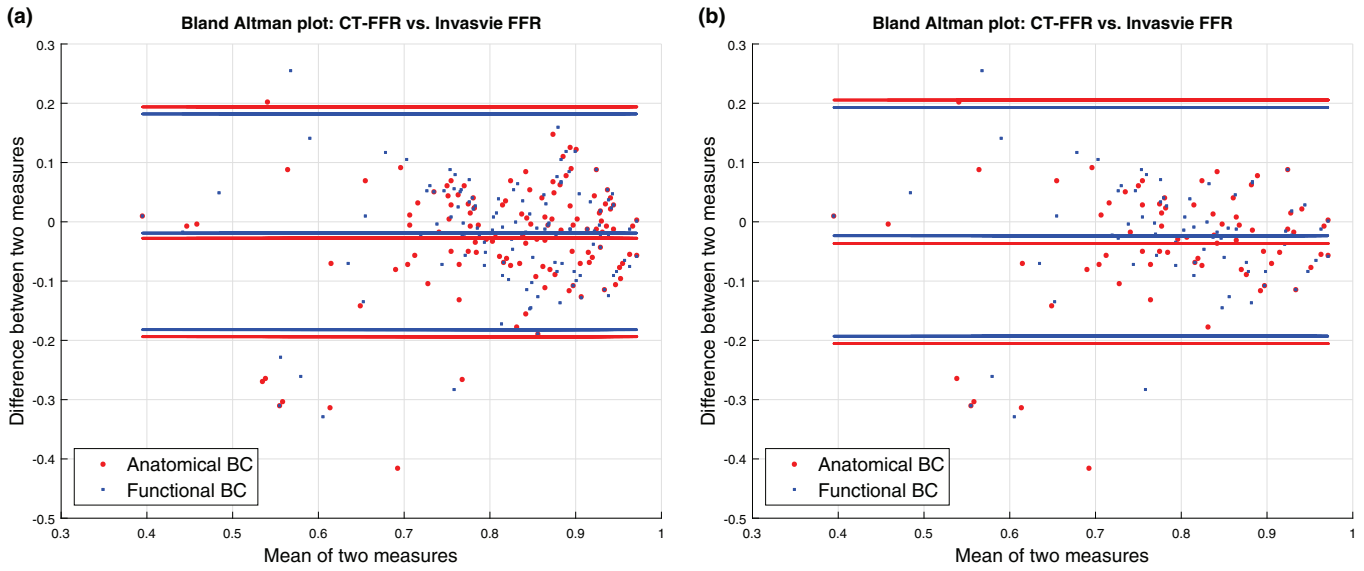

FIG. 3. Bland–Altman plot of the estimated CT-FFR values vs invasively measured FFR values for all lesions (N = 123, (a)) and for intermediate lesions (CCTA DS stenosis 30%–70%) (N = 72, (b)) using the anatomically personalized (circles) and functionally personalized (squares) boundary condition models. The functionally personalized model reduced the overall bias by ~30% and the 95% limits of agreement by 6% compared to the anatomically personalized model.

30% and the 95% limits of agreement by 6% compared to the anatomically personalized model. In the assessment of only the intermediate lesions, the functionally personalized BC model reduces the overall bias by 36% and the 95% limits of agreement by 6% compared to the anatomically personalized BC model.

The ratio of true positive CT-FFR with the functional BC model was 31.7% (39 of 123 lesions), true negative 50.4% (62 of 123 lesions), false positive 12.2% (15 of 123 lesions), and false negative 5.7% (7 of 123 lesions). The ratio of true positive CT-FFR with the anatomical BC model was 31.7% (39 of 123 lesions), true negative 50.4% (62 of 123 lesions), false positive 12.2% (15 of 123 lesions), and false negative 5.7% (7 of 123 lesions).

In the assessment of only the intermediate lesions, the ratio of true positive CT-FFR with the functional BC model was 41.7% (30 of 72 lesions), true negative 41.7% (30 of 72 lesions), false positive 11% (8 of 72 lesions), and false negative 5.6% (4 of 72 lesions). The ratio of true positive CT-FFR with the anatomical BC model was 41.7% (30 of 72 lesions), true negative 40.3% (29 of 72 lesions), false positive 12.5% (9 of 72 lesions), and false negative 5.6% (4 of 72 lesions).

Table II summarizes the performance metrics of the simulated CT-FFR values compared to invasively measured FFR values with clinical threshold of FFR $\leq$ 0.8 indicating hemodynamically significant lesions. The functionally personalized BC model improved both estimation metrics (RMSE, bias, and limits of agreement) and clinically relevant metrics (specificity, positive/negative predictive value, and area under the curve [AUC]) compared to the anatomically personalized BC model when assessing both the entire set of lesions and in an independent assessment of only the intermediate lesions. However, the improvements did not reach the level of statistical significance in the study population.

Figure 4 depicts the flow simulation results of a patient with an intermediate DS (54%) and hemodynamically significant lesion (invasive FFR = 0.67) along the left anterior descending (LAD) artery obtained with the anatomically personalized BC model [Fig. 4(b)] and with the functionally personalized BC model [Fig. 4(c)]. In this case, the CT-FFR value obtained with the anatomically personalized model overestimated the severity of the lesion substantially (CT-FFR = 0.41), while the CT-FFR value estimated using the functionally personalized BC model reduced the lesion's severity overestimation by ~27% (CT-FFR = 0.60).

Figure 5 depicts flow simulation results of a coronary tree of a patient with an intermediate but hemodynamically nonsignificant lesion (DS = 38%, invasive FFR = 0.92) along the LAD obtained with the anatomically personalized BC model [Fig. 5(b)] and with the functionally personalized BC model [Fig. 5(c)]. In this case, the CT-FFR values obtained with both the anatomically and functionally personalized models were similar (CT-FFR = 0.93) and in good agreement with the invasive FFR measurement (FFR = 0.92). The agreement between the two models represents a normal pressure drop in the coronary outlet, which did not initiate the microvasculature resistance autoregulation mechanism.

4. DISCUSSION

Our study demonstrates the possibility to account for autoregulation mechanisms controlling the coronary microvascular resistance in hemodynamic significance assessment based on flow simulations.

Coronary computed tomography angiography has a high negative predictive value in eliminating CAD. However, CCTA's specificity in detecting hemodynamically significant

TABLE II. Performance metrics of the simulated CT-FFR values compared to invasively measured FFR values with clinical threshold of FFR ≤ 0.8 indicating a hemodynamically significant lesion. Top row for intermediate lesions only (N = 72), and bottom row for entire set of lesions (N = 123). Improved performance of the functionally personalized BC model in bold.

	RMSE	Sensitivity	Specificity	Positive predictive value	Negative predictive value	Area under the curve	Bias	Limits of Agreement
Intermediate lesions (N = 72)								
Functional BC	0.099	0.882 [95% CI: 0.765–0.971]	0.79 [95% CI: 0.658–0.921]	0.79 [95% CI: 0.724–0.856]	0.882 [95% CI: 0.827–0.937]	0.909 [95% CI: 0.841–0.975]	0.023	0.189
Anatomical BC	0.108	0.882 [95% CI: 0.765–0.971]	0.763 [95% CI: 0.631–0.895]	0.769 [95% CI: 0.702–0.836]	0.879 [95% CI: 0.822–0.936]	0.898 [95% CI: 0.823–0.97]	0.036	0.201
Improvement (%)	**9**	0	**3**	**3**	**0.4**	**1**	**36**	**6**
All lesions (N = 123)								
Functional BC	0.093	0.848 [95% CI: 0.739–0.935]	0.805 [95% CI: 0.714–0.896]	0.722 [95% CI: 0.633–0.827]	0.899 [95% CI: 0.833–0.956]	0.884 [95% CI: 0.834–0.942]	0.02	0.176
Anatomical BC	0.1	0.848 [95% CI: 0.739–0.935]	0.805 [95% CI: 0.714–0.896]	0.722 [95% CI: 0.633–0.816]	0.899 [95% CI: 0.836–0.956]	0.875 [95% CI: 0.81–0.935]	0.03	0.188
Improvement (%)	**7.9**	0	**1.6**	**1.7**	**0.2**	**1**	**30**	**6**

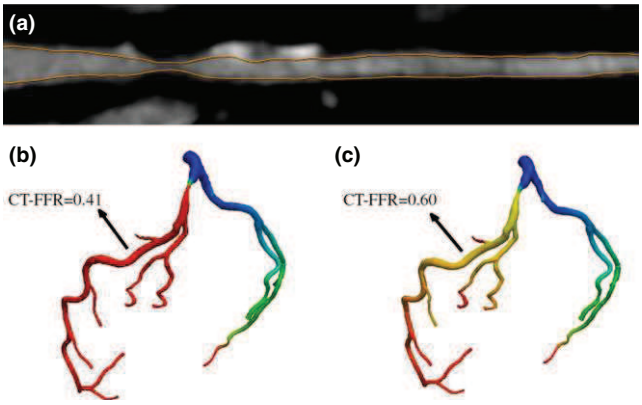

FIG. 4. Flow simulation results of a patient with an intermediate DS (54%) and hemodynamically significant lesion (invasive FFR = 0.67) along the left anterior descending (LAD) artery (a), obtained with the anatomically personalized BC model (b) and with the functionally personalized BC model (c). CT-FFR value obtained with the anatomically personalized model overestimated the severity of the lesion substantially (CT-FFR = 0.41), while the CT-FFR value estimated using the functionally personalized BC model reduced the lesion's severity overestimation by ~27% (CT-FFR = 0.60).

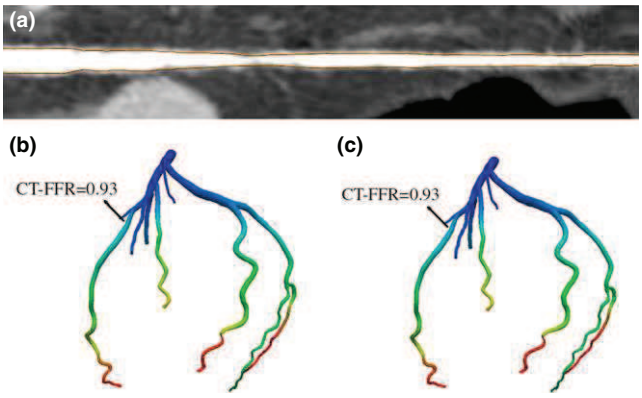

FIG. 5. Flow simulation results of a coronary tree of a patient with an intermediate but hemodynamically nonsignificant lesion (DS = 38%, invasive FFR = 0.92) along the LAD (a) obtained with the anatomically personalized BC model (b) and with the functionally personalized BC model (c). CT-FFR values obtained with both anatomically- and functionally personalized models were similar (CT-FFR = 0.93) and in good agreement with the invasive FFR measurement. The agreement between the two models represents a normal pressure drop in the coronary outlet, which did not initiate the microvascular resistance autoregulation mechanism.

CAD is limited, mainly due to its inability to provide a functional characterization of the coronary lesions.

Several approaches were suggested to improve CCTA specificity in assessing the hemodynamic significance of coronary lesions by means of FFR. Choi et al.[24] and Stuijfzand et al.[25] proposed to use the transluminal attenuation gradient (TAG) to determine the hemodynamic significance of a coronary lesion. Wang et al.[26,27] analyzed the benefit of lesion-specific properties including lesion length/minimal luminal diameter in addition to TAG and corrected coronary attenuation in addition to CCTA-based stenosis estimates in predicting the hemodynamic significance of coronary lesions.

Itu et al.[28] proposed a deep neural network framework to estimate the FFR values from CCTA data by extracting local geometrical features for each point in the coronary tree combined with upstream and downstream geometrical features.

Recent comparative studies suggested that physics-based CT-FFR has a better receiver operating characteristics (ROC)-AUC for prediction of the hemodynamic significance of coronary lesions than the TAG and the lesion geometry-based approaches with invasive FFR as the reference.[26,29]

The accuracy of physics-based flow simulation of blood flow in the coronary arteries is dependent upon several factors. A major factor is the accurate modeling of the coronary lumen tree.[30] While there is still room for improvement in this direction, we tried to minimize the impact of lumen estimation error by using the lumen segmentation algorithm developed by Freiman et al.[6] to account specifically as much as possible for the uncertainty in lumen cross-sectional area estimation.

An additional factor is the accurate modeling of boundary conditions required for the simulation, including autoregulatory mechanisms controlling the influence of different factors on the overall flow. For example, Min et al.[9] used the inlet flow and the outlet resistance as boundary conditions. They calculated the inlet flow as a function of the myocardial mass and blood pressure, and used the 3D coronary tree model to distribute the overall microvascular resistance to the coronary tree outlets that is inversely proportional to the coronary outlet radii following the physiological principles described by Huo and Kassab.[13] Sharma et al.[14] first calculated a personalized overall resistance at the rest state of the cardiac cycle as a function of the myocardial mass and inlet pressure, and then derived the target resistance at hyperemia using a transfer function modeling the vasodilation phenomenon. Recently, Ko et al.[16] suggested the use of the structural deformation of coronary lumen and aorta during the cardiac cycle to determine the boundary condition.

Several physiological studies demonstrated an autoregulation mechanism adjusting the microvascular resistance in response to reduced pressure in the coronary outlet. For example, Jayaweera et al.[18] suggested microvascular resistance modifications as a response to flow-limiting stenosis in animal studies, Verhoeff et al.[19] demonstrated an autoregulated reduction in microvascular resistance as a response to decreased pressure at the coronary outlet in 24 human subjects, and Chamuleau et al.[20] showed a positive association between coronary lesion severity and variability in distal microvascular resistance that normalizes after angioplasty.

In this work, we presented a functionally personalized boundary condition model for CT-FFR that accounts specifically for this functional dependency by first determining the pressure drop at the coronary tree outlets, and then adjusting the microvascular resistance at the coronary outlet according to the associated pressure drop.

The quantitative CTA analysis presented in the study was done retrospectively and did not influence the clinical decision to refer patients after CTA to an invasive exam. The clinical decision was driven by qualitative interpretation of the CTA data by the interpreting physician and clinical symptoms.

Our functionally personalized BC model slightly improved CT-FFR specificity in determining hemodynamic significance lesions, compared to the anatomically personalized model (sensitivity/specificity: 0.833/0.798 vs 0.833/0.786) in our entire dataset of 123 coronary lesions with invasive FFR measurements as the reference. Likewise, specific analysis of lesions with intermediate diameter stenosis (30%–70%, N = 72), also showed that the functionally personalized BC model improved CT-FFR specificity in determining hemodynamic significance lesions, compared to the anatomically personalized model (sensitivity/specificity: 0.882/0.79 vs 0.882/0.763).

As demonstrated in Fig. 4, the highest impact of our model is in patients with low FFR values. In such cases our model has the potential to reduce the overestimation of the hemodynamic impact of the lesion's severity.

Our study has several limitations: First, the study was a retrospective study by design and was limited to datasets obtained with CT scanners from the same vendor. This may limit the potential generalization of our approach to other patient populations and data acquired with different CT scanners. A more comprehensive study including prospective data collection of CCTA data acquired by scanners from multiple vendors is desired to assess the full potential of functionally personalized BC models in assessing the hemodynamic significance of coronary lesions.

Second, we used a 0D lumped model to estimate coronary pressure, and model the coronary blood flow as an incompressible, Newtonian fluid with laminar flow. While previous studies show that these approaches can provide accurate CT-FFR estimates similar to CFD approaches,[12] additional experiments using CFD computations might be of interest before generalizing the proposed approach to other CT-FFR computation models. In addition, a more accurate blood flow model may provide an additional level of improvement.

Third, we limited the model to rely on data only available in the CCTA exam. As a result, some of the parameters such as blood pressure was assumed to be the same across the entire patient population. Including additional patient-specific data may have the potential to provide further personalization and may result in improved CT-FFR clinical performance. Moreover, similar to other CT-FFR methods, our approach relies upon accurate segmentation of the coronary arteries from the CCTA data. This is still a challenging task due to limited image resolution and potential imaging artifacts. Our results show that some outliers still exist and may be attributed to imaging artifacts that cause inaccurate segmentation of the coronaries.

Finally, due to the limited data availability, we evaluated our BC model using a k-fold cross-validation approach. A larger study involving large amount of datasets divided into training and testing groups has the potential to better demonstrate the potential of the functionally personalized BC model

in improving overall CT-FFR estimates for CCTA-based hemodynamic significance assessment of CAD.

In conclusion, we have presented a functionally personalized boundary condition model for physics-based flow simulations that accounts specifically for autoregulation mechanism controlling the coronary microvascular resistance. We demonstrated the benefit of accounting for autoregulation in assessing the hemodynamic significance of coronary lesions. The proposed algorithm has the potential to facilitate CCTA-based hemodynamic significance assessment of CAD in clinical routine.

CONFLICTS OF INTEREST

M.F., M.V., and L.G. are employees of Philips Healthcare. H.N., S.P., and H.S. are employees of Philips Research.

[a)]Author to whom correspondence should be addressed. Electronic mail: moti.freiman@philips.com

REFERENCES

1. Murray CJL. GBD 2015 mortality and causes of death collaborators. Global, regional, and national age–sex specific all-cause and cause-specific mortality for 240 causes of death, 1990–2013: a systematic analysis for the Global Burden of Disease Study 2013. *Lancet*. 2015;385:117–171.
2. Scot-heart T. CT coronary angiography in patients with suspected angina due to coronary heart disease (SCOT-HEART): an open-label, parallel-group, multicentre trial. *Lancet*. 2015;385:2383–2391.
3. Meijboom WB, van Mieghem CAG, van Pelt N, et al. Comprehensive assessment of coronary artery stenoses. Computed tomography coronary angiography versus conventional coronary angiography and correlation with fractional flow reserve in patients with stable angina. *J Am Coll Cardiol*. 2008;52:636–643.
4. Coenen A, Lubbers MM, Kurata A, et al. Fractional flow reserve computed from noninvasive CT angiography data: diagnostic performance of an on-site clinician-operated computational fluid dynamics algorithm. *Radiology*. 2015;274:674–683.
5. Nørgaard BL, Leipsic J, Gaur S, et al. Diagnostic performance of noninvasive fractional flow reserve derived from coronary CT angiography in suspected coronary artery disease: the NXT trial. *J Am Coll Cardiol*. 2014;63:1145–1155.
6. Freiman M, Nickisch H, Prevrhal S, et al. Improving CCTA-based lesions' hemodynamic significance assessment by accounting for partial volume modeling in automatic coronary lumen segmentation. *Med Phys*. 2017;44:1040–1049.
7. Kirişli HA, Schaap M, Metz CT, et al. Standardized evaluation framework for evaluating coronary artery stenosis detection, stenosis quantification and lumen segmentation algorithms in computed tomography angiography. *Med Image Anal*. 2013;17:859–876.
8. Lugauer F, Zheng Y, Hornegger J, Kelm BM. Precise lumen segmentation in coronary computed tomography angiography. In: *Lecture Notes in Computer Science (Including Subseries Lecture Notes in Artificial Intelligence and Lecture Notes in Bioinformatics)*. Vol 8848.; 2014:137–147.
9. Min JK, Taylor CA, Achenbach S, et al. Noninvasive fractional flow reserve derived from coronary CT angiography clinical data and scientific principles. *JACC Cardiovasc Imaging*. 2015;8:1209–1222.
10. Giannopoulos A, Tang A, Ge Y, et al. Diagnostic performance of a lattice boltzmann-based method for fast CT-fractional flow reserve. *EuroIntervention*. 2017. https://doi.org/10.4244/EIJ-D-17-00019.
11. Itu L, Sharma P, Mihalef V, Kamen A, Suciu C, Lomaniciu D. A patient-specific reduced-order model for coronary circulation. In: 2012 9th IEEE International Symposium on Biomedical Imaging (ISBI).; 2012:832–835.
12. Nickisch H, Lamash Y, Prevrhal S, et al. Learning patient-specific lumped models for interactive coronary blood flow simulations. In: Navab N, Hornegger J, Wells MW, Frangi FA, eds. *Medical Image Computing and Computer-Assisted Intervention – MICCAI 2015: 18th International Conference, LNCS*, Vol. 9350. Vol 9350. Springer International Publishing; 2015:433–441.
13. Huo Y, Kassab GS. Intraspecific scaling laws of vascular trees. *J R Soc Interface*. 2012;9:190–200.
14. Sharma P, Itu L, Zheng X, et al. A framework for personalization of coronary flow computations during rest and hyperemia. In: Proceedings of the Annual International Conference of the IEEE Engineering in Medicine and Biology Society, EMBS.; 2012:6665–6668.
15. Kishi S, Giannopoulos AA, Tang A, et al. Fractional flow reserve estimated at coronary CT angiography in intermediate lesions: comparison of diagnostic accuracy of different methods to determine coronary flow distribution. *Radiology*. 2017:162620.
16. Ko BS, Cameron JD, Munnur RK, et al. Noninvasive CT-Derived FFR based on structural and fluid analysis: a comparison with invasive FFR for detection of functionally significant stenosis. *JACC Cardiovasc Imaging*. 2017;10:663–673.
17. Kim HJ, Jansen KE, Taylor CA. Incorporating autoregulatory mechanisms of the cardiovascular system in three-dimensional finite element models of arterial blood flow. *Ann Biomed Eng*. 2010;38:2314–2330.
18. Jayaweera AR, Wei K, Coggins M, et al. Role of capillaries in determining CBF reserve: new insights using myocardial contrast echocardiography. *Am J Physiol*. 1999;277:H2363–H2372.
19. Verhoeff B-J, Siebes M, Meuwissen M, et al. Influence of percutaneous coronary intervention on coronary microvascular resistance index. *Circulation*. 2005;111:76–82.
20. Chamuleau SAJ, Siebes M, Meuwissen M, Koch KT, Spaan JAE, Piek JJ. Association between coronary lesion severity and distal microvascular resistance in patients with coronary artery disease. *Am J Physiol Heart Circ Physiol*. 2003;285:H2194–H2200.
21. Pedley TJ. *The Fluid Mechanics of Large Blood Vessels*. Cambridge, UK: Cambridge University Press; 1980.
22. Muzychka YS, Yovanovich MM. Pressure drop in laminar developing flow in noncircular ducts: a scaling and modeling approach. *J Fluids Eng*. 2009;131:111105.
23. Truckenbrodt E. *Fluidmechanik*. Berlin: Springer-Verlag; 1980.
24. Choi JH, Min JK, Labounty TM, et al. Intracoronary transluminal attenuation gradient in coronary CT angiography for determining coronary artery stenosis. *JACC Cardiovasc Imaging*. 2011;4:1149–1157.
25. Stuijfzand WJ, Danad I, Raijmakers PG, et al. Additional value of transluminal attenuation gradient in CT angiography to predict hemodynamic significance of coronary artery stenosis. *JACC Cardiovasc Imaging*. 2014;7:374–386.
26. Wang R, Renker M, Schoepf UJ, et al. Diagnostic value of quantitative stenosis predictors with coronary CT angiography compared to invasive fractional flow reserve. *Eur J Radiol*. 2015;84:1509–1515.
27. Wang R, Baumann S, Schoepf UJ, et al. Comparison of quantitative stenosis characteristics at routine coronary computed tomography angiography with invasive fractional flow reserve for assessing lesion-specific ischemia. *J Cardiovasc Comput Tomogr*. 2015;9:546–552.
28. Itu L, Rapaka S, Passerini T, et al. A machine-learning approach for computation of fractional flow reserve from coronary computed tomography. *J Appl Physiol*. 2016;121:42–52.
29. Ko BS, Wong DTL, Nørgaard BL, et al. Diagnostic performance of transluminal attenuation gradient and noninvasive fractional flow reserve derived from 320–Detector Row CT angiography to diagnose hemodynamically significant coronary stenosis: an NXT substudy. *Radiology*. 2016;279:75–83.
30. Huo Y, Svendsen M, Choy JS, Zhang Z-D, Kassab GS. A validated predictive model of coronary fractional flow reserve. *J R Soc Interface*. 2012;9:1325–1338.